NJC

Accepted Manuscript

This article can be cited before page numbers have been issued, to do this please use: J. E. Martínez Porcel, M. B. Rivas Aiello, V. B. Arce, D. Di Silvio, S. E. Moya and D. Martire, *New J. Chem.*, 2019, DOI: 10.1039/C9NJ01013K.

ROYAL SOCIETY OF CHEMISTRY

rsc.li/njc

DOI: 10.1039/C9NJ01013K

Effect of Hybrid SiO_2@Ag Nanoparticles with Raspberry-like Morphology on the Excited States of the Photosensitizers Rose Bengal and Riboflavin.

Joaquín E. Martínez Porcel[a,b], María Belén Rivas Aiello[a], Valeria B. Arce[c], Desire Di Silvio[b], Sergio E. Moya[b] and Daniel O. Mártire*[,a]

[a] Instituto de Investigaciones Fisicoquímicas Teóricas y Aplicadas (INIFTA), Universidad Nacional de La Plata, Diag 113 y 64, La Plata, Argentina. E-mails: JEMP: jmartinezporcel@inifta.unlp.edu.ar; MBRA: belenra@inifta.unlp.edu.ar

[b] Soft Matter Nanotechnology, Centre for Cooperative Research in Biomaterials, CICbiomaGUNE Unidad Biosuperficies, Paseo Miramon 182 Edif C, 20009 San Sebastian, Spain. E-mails: SM: smoya@cicbiomagune.es; DDS: ddisilvio@cicbiomagune.es

[c] Centro de Investigaciones Ópticas (CIOp), (CONICET La Plata - CIC - UNLP), Cno. Parque Centenario e/ 505 y 508, Gonnet, Argentina. E-mail: VA: varce@ciop.unlp.edu.ar

Corresponding Author

*Tel: +54 221 4257430. Fax: +54 221 4254642. E-mail: dmartire@inifta.unlp.edu.ar

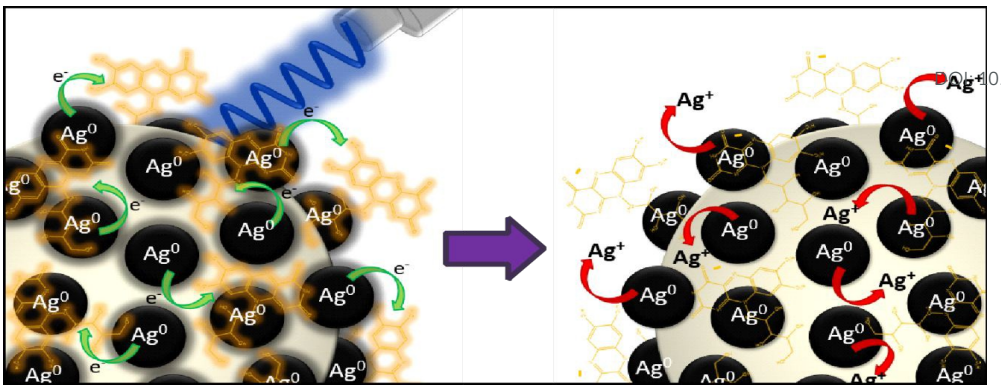

ABSTRACT

Metal nanoparticles (NPs) can strongly affect the photophysics of organic molecules through different mechanisms. To investigate the effect of silver nanomaterials on the triplet state dynamics of the photosensitizers Riboflavin (Rf) and Rose Bengal (RB^{2-}), we have here synthesized core-shell silica silver nanoparticles with raspberry-like morphology (SiO_2@Ag NPs). For the synthesis of SiO2@Ag NPs from SiO_2 nanoparticles a new combination of reported strategies was employed. The synthetic methodology involves in a first step $SnCl_2$ as a precursor to obtain a homogeneous deposition of silver nuclei on colloidal silica spheres. In a second step, the growth of the silver nanoparticles is mediated by the photochemically generated ketyl radical of the substituted benzoin Irgacure-2959 (I-2959). Both Rf and RB^2 dyes are adsorbed on the nanoparticles. Transient absorption spectroscopy experiments showed that there is a charge transfer process from the excited state of the adsorbed Rf to the silver nanoparticles. However, no similar reaction is observed for RB^{2-}. These results are explained in terms of the expected equilibrium constants of the electron transfer for both dyes.

INTRODUCTION

Collective oscillations of electrons in metal nanostructures or a localized surface plasmon resonance (LSPR) can strongly affect the dynamics of the singlet and triplet excited states of organic molecules.[1,2] Due to their LSPRs, metal nanoparticles (NPs) can intensely interact with adjacent organic molecules by different mechanisms, including electron transfer, energy transfer, and by affecting both radiative and nonradiative deactivation processes of excited states of the organic molecules.[3,4] Pacioni et al. reported the enhancement of the quantum yield of the triplet state of methylene blue by gold NPs.[2] The increase of the triplet quantum yields of organic photosensitizers in the neighborhood of metal nanoparticles (NPs) can lead to the so called metal-enhanced production of singlet oxygen, which can be applied for tumor treatment in photodynamic therapy.[5]

In a recent paper of our group[6] we have shown that in the presence of pectin-coated silver nanoparticles a Riboflavin-Ag complex increases the triplet state population of the flavin. As a consequence, higher concentrations of singlet oxygen and superoxide radical anion are formed in aerated solutions. We have also observed in HeLa cells a higher phototoxicity of the photosensitizer when complexed with the nanoparticles, as an indirect result of the enhanced triplet state population of the flavin.[7]

In this line, we have here prepared and characterized core-shell silica silver nanoparticles with raspberry-like morphology (SiO_2@Ag NPs). This nanomaterial has been chosen for two main reasons: (a) The surface of the nanoparticles presents exposed silanol groups from SiO_2, which can potentially act as sites for the adsorption of organic molecules.[8] (b) At the same time the Ag nanoparticles supported by the silica are in proximity with the dye. The silica support acts as a mean to immobilize both the metal NP and the dye in a close range. This nanomaterial also offers the possibility of performing comparative experiments with silica nanoparticles without silver shell (SiO_2NP) in order to corroborate whether the observed effects of SiO_2@AgNP on the photophysics of the photosensitizers are due to the metal and not only to the immobilization of the dyes on the silica surface.

For the synthesis of SiO_2@Ag NPs from SiO_2 nanoparticles a new combination of reported strategies was employed. (Figure 1). This method involves in the first two steps the homogeneous deposition of silver nuclei on colloidal silica spheres as reported by the group of Liz-Marzán.[9] In this procedure SiO_2 NPs were treated with $SnCl_2$ in acid medium to yield SiO_2@Sn^{2+} NPs, which have Sn^{2+} ions adsorbed on their surface. The Sn^{2+} ions reduce Ag^+ ions, and superficial Ag nuclei (seeds) are generated, resulting in SiO_2@nucAg NPs. For the growth of Ag nanoparticles from seeds the photochemical method reported by the group of Scaiano[10] was applied. This method has many advantages since it is a room temperature procedure, which combines the characteristic features of light activation i.e. versatility and convenience of the process, high spatial resolution and reaction controllability (intensity and wavelength).[11]

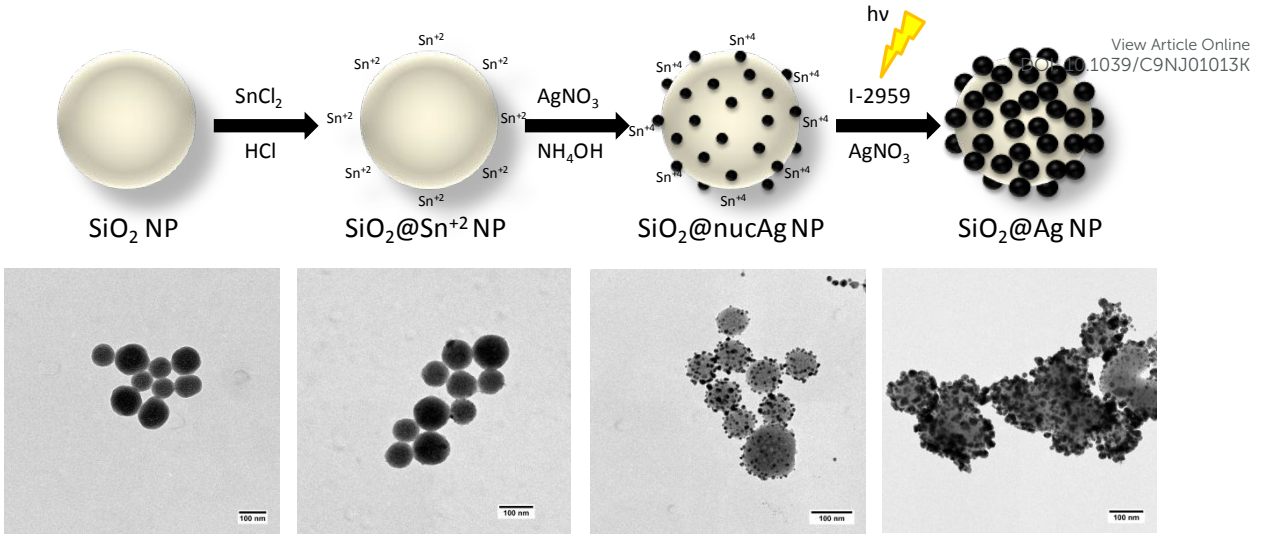

Figure 1: Top: Synthesis of SiO_2@Ag NPs from SiO_2 NPs. Bottom: TEM micrographs of the nanoparticles obtained in each synthesis step.

This latter procedure consists in the photogeneration of ketyl radicals (reaction 1), produced by photolysis of the substituted benzoin Irgacure-2959 (I-2959), which induce the reduction of Ag^+ ions to metallic silver.

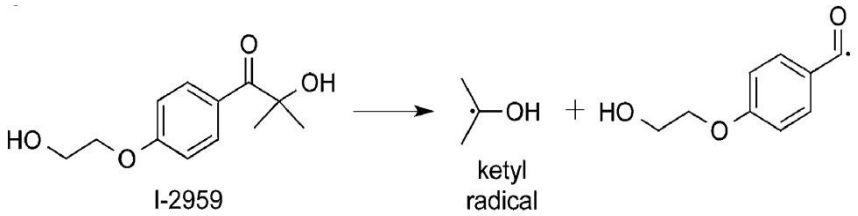

(1)

The colloidal nanoparticles produced at different stages during synthesis were analyzed by zeta potential (ξ) measurements, transmission electron microscopy (TEM), and X-ray photoelectron spectroscopy (XPS).

We will investigate here the interaction of SiO_2@Ag NPs with the excited states of two photosensitizers: the anionic form of Rose Bengal (RB^{2-}) and the neutral Riboflavin molecule (Rf). These two photosensitizers have been chosen because of their potential in photodynamic therapy. [12,13,14]

EXPERIMENTAL SECTION

View Article Online
DOI: 10.1039/C9NJ01013K

Materials. Silver nitrate, Sodium Hydroxide, Tin (II) Chloride, I-2959, TEOS, Riboflavin and Rose Bengal were purchased from Sigma-Aldrich. Ammonium Hydroxide and Hydrochloric acid were obtained from Acros Organics, and Absolute Ethanol from Scharlau. All experiments were performed with deionized water.

Synthesis of SiO_2 NPs. Colloidal silica particles were prepared by the well-known Stöber method.[15] Briefly, 3mL of 30% w/v aqueous ammonia and 50 mL of absolute alcohol were mixed in an Erlenmeyer flask. Then, 1.5 mL of tetraethyl orthosilicate (TEOS) was added quickly under stirring. Gentle stirring was continued overnight. Under these conditions 100 nm-diameter nanoparticles should be formed.[16] The solvent was then exchanged by centrifugation at 7000-9000 rpm for 30 min, removing the supernatant and adding water. This procedure was repeated a second time to complete the solvent exchange. The solvent was then evaporated to dryness and the solid stored at room temperature.

Synthesis of SiO_2@Sn^{2+} NPs. SiO_2 NPs (10 mg) were resuspended in 10 mL of a 0.02% w/v NaOH solution and then 10 mL of a 3 % w/v $SnCl_2$ solution in 1 M HCl was added. The mixture was stirred for 2 h, and then centrifuged at 7000-9000 rpm for 10 min. The supernatant was separated and the precipitate was washed 3 times with ultrapure water. In some experiments a lower concentration of $SnCl_2$ (1.0 % w/v) was employed. These nanoparticles were also treated to yield SiO_2@nucAg NPs and SiO_2@Ag NPs, as indicated in the following paragraphs.

Synthesis of SiO_2@nucAg NPs. The SiO_2@Sn^{+2} NPs were resuspended in a 0.35 M ammoniac $AgNO_3$ solution and the mixture was stirred for 2 h. Then, after centrifugation at 7000-9000 rpm for 10 min, the supernatant was separated and the precipitate was washed 3 times with water.

Synthesis of SiO_2@Ag NPs. The SiO_2@nucAg NPs were resuspended in 20 mL of ultrapure water in a quartz tube containing 3.4 mg of $AgNO_3$ and 4.5 mg of I-2959. The colloidal suspension was irradiated for 15 min in a Rayonet RPR-100 reactor equipped with 8 RPR-2537A lamps. The supernatant was separated after centrifugation at 7000-9000 rpm for 10 min. The precipitate was resuspended in 20 mL of ultrapure water. The colloidal suspension obtained displays a yellow-red brownish color.

Most experiments were performed with SiO_2@Sn^{2+} NPs, SiO_2@nucAg NPs, SiO_2@Ag NPs prepared employing the highest concentration of $SnCl_2$ (3 % w/v). When the 1.0 % w/v $SnCl_2$ was used to obtain the tin precursor, the resulting silver- coated silica nanoparticles were named SiO_2@Ag-low NPs to indicate the lower silver coverage achieved.

Transmission Electron Microscopy (TEM). Transmission electron microscopy images were acquired by using a JEOL JEM 1010 microscope operating at an acceleration voltage of 120 kV. Carbon films supported on 400 mesh copper grids

were used. 5 μL of undiluted suspension with SiO_2, SiO_2@nuncAg, SiO_2@Ag-low and SiO_2@Ag NPs were transferred to grids and incubated for 1 min. The excess of the suspension was removed with a paper filter.

Dynamic Light Scattering and ζ-potential. Dynamic Light Scattering measurements were carried out with a ζ-Sizer Malvern Instrument in backscattering mode. All studies were performed at a 173° scattering angle with temperature controlled at 25 °C in 1 mL polystyrene cuvettes. The NPs were characterized in terms of hydrodynamic diameter and ζ-potential. For DLS short time measurements were carried out for a total of 15 min, with 3 consecutive measurements for each sample. ζ-potential measurements were performed in auto-mode at 25 °C, with 3 consecutive measurements at different pH values.

Silver amount determination by ICP. In order to determine the silver content of the nanoparticles, 0.5 mL of the samples were digested with 0.5 mL of concentrated HNO_3 for 24 h. Then, water was added to a final volume of 10 mL. The resulting solutions were analyzed by Inductively Coupled Plasma Emission Spectroscopy (ICPE) with a Shimadzu ICPE-9800 equipment. From now on, the concentration of Ag will be specified instead of that of the nanoparticles containing Ag.

Fluorescence Spectroscopy. Fluorescence measurements were carried out with a HORIBA JOBIN-YVON Spex Fluorolog FL3-11. For steady-state measurements the excitation wavelength was 355 nm.

Fluorescence Correlation Spectroscopy (FCS). FCS experiments were performed with a Confocal Microscope ZeissNLO 880 (Carl Zeiss Gmbh). Acquisition and analysis are controlled by Zen black software. Argon laser at 458 nm and the HeNe laser at 633 nm were used as excitation sources. GaASP and PTM detectors were used for single molecules fluorescence detection and dynamic characterization. Measurements were performed with a Zeiss C-Apochromat 40, NA 1.2 water immersion objective. 1 mL of dispersion were measured in Lab-Tek Q5 Chambered Coverglass (Thermo Fisher Scientific). QuickFit 3.0 free software was used for FCS data analysis.

Laser Flash-Photolysis (LFP). An LP980 laser flash-photolysis from Edinburgh instruments was employed. The third harmonic (355 nm) of a Continuum Surelite Nd:YAG laser (20 ns fwhm) was employed as excitation source (1 Hz, 10 mJ/pulse). Since several species contribute to the absorption traces, a global analysis of the transient absorption data was carried out. Decay-associated difference spectra (DADS) were performed with the free software program Glotaran.[17]

RESULTS AND DISCUSSION

Synthesis and characterization of SiO_2@Ag NPs. The average hydrodynamic diameter of SiO_2@Ag NPs obtained from DLS measurements was 133 ± 86 nm. An additional peak in the intensity distribution, which accounts for less than 3% of the overall scattered light, was also detected. The large average hydrodynamic diameter of this peak, 4.6 µm, indicates aggregation (see Figure S1 in the Supplementary Material).

The composite nanomaterials at the different steps of synthesis (Figure 1) were examined by TEM, DLS, XPS and Zeta potential.

The TEM micrographs for SiO_2@nucAg and SiO_2@Ag NPs (Figure 1) show discontinuous and random deposits of nanosilver (as shown by small darker spheres) on silica surfaces, confirming the formation of core-shell silica-silver nanoparticles with raspberry-like morphology.

The size distribution histogram of SiO_2 NPs obtained from TEM images shows a NP population with a diameter of 85 ± 15 (Figure 2). The average size of the Ag nanoparticles on the surface of SiO_2@Ag NPs is 7 ± 3 nm (Figure 2). TEM images of SiO_2@Ag-low NPs with a lower silver coverage on the SiO_2 spheres is shown in Figure S2 (Supplementary Material).

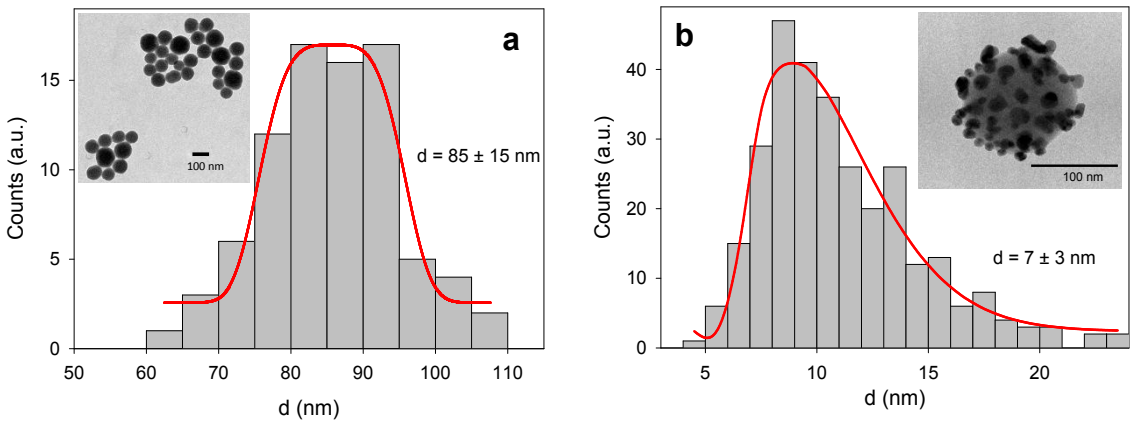

Figure 2: Size distribution histograms of: (a) SiO_2 NPs, (b) Ag NPs on the surface of SiO_2@Ag NPs. The insets correspond to characteristic TEM images of the NPs.

Dynamic light scattering experiments yielded hydrodynamic radii in complete agreement with TEM results (see Electronic Supporting Information Figure S1).

View Article Online
DOI: 10.1039/C9NJ01013K

Figure 3 shows the pH-dependence of the zeta potential (ζ) of the NPs generated at each synthesis step, i.e., SiO_2, SiO_2@Sn^{2+}, SiO_2@nucAg, and SiO_2@Ag NPs. Negative values of ζ were measured for the SiO_2 NPs in the whole pH range of analysis (4 - 12), as a result of deprotonation of surface silanols.[18] In contrast, for SiO_2@Sn^{2+} a point of zero charge of ca. 4.5 was obtained. Since at this pH the ζ measured for SiO_2 was negative, the zero charge measured after Sn^{+2} complexation is indicative of the successful surface adsorption of Sn^{2+} ions on the silica nanoparticles.

The values of ζ for SiO_2@nucAg and SiO_2@Ag were also negative in the pH range 4 - 12, in line with the negative contribution to ζ of the silanol groups and the negative zeta potential of silver nanoparticles above pH 8.[19]

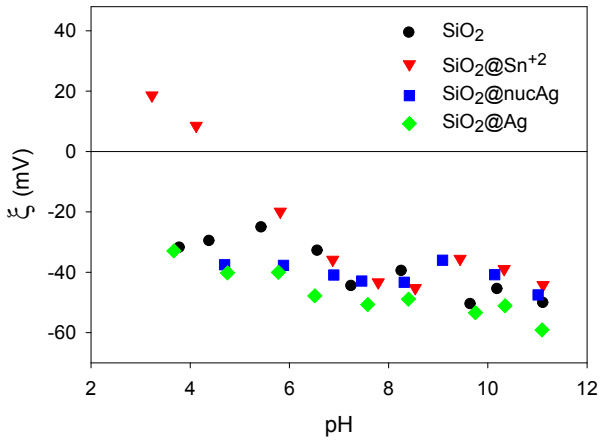

Figure 3: Zeta potential (ζ) dependence on pH for the suspensions of the nanoparticles obtained during the different synthesis stages.

Figure S3 (Supplementary Material) shows the evolution of the XPS spectra of silica spheres during the successive synthesis steps. Deconvolution of the XPS spectra of SiO_2, SiO_2@Sn^{+2}, and SiO_2@nucAg shows Si2p peaks in the 101 - 102 eV range (Table 1), which are characteristic of Si^{2+} and Si^{3+} present in S_xO_y suboxides.[20],[21]Additionally, Si2p peaks in the 101-102 eV region were also assigned to SiO_xC_y species.[22]However, the sample SiO_2@Ag, which was photoirradiated at 253.7 nm, shows the characteristic Si2p signal of SiO_2 at 103.5 eV.[21,23]. Aminuzzaman et al.[23] reported that after exposure

to 254 nm light, the Si2p peak of polysilsesquioxane films shifts from 102.22 eV to 103.50 eV. Their results were explained considering a chemical conversion from a T cage moiety of polysilsesquioxane to SiO_2.

Table 1. Detail of the XPS Si2p and O1s peaks obtained by deconvolution of the experimental signals.

	Peak 1(eV)	Area (%)	Peak2 (eV)	Area (%)	Peak3 (eV)	Area (%)
Si 2p						
SiO_2	102.0	83.9	101.8	16.1	---	---
SiO_2@Sn^{+2}	101.9	97.8	101.4	2.2	---	---
SiO_2@nucAg	101.2	100	---	---	---	---
SiO_2@Ag	103.5	84.3	103.2	15.7	---	---
O 1s						
SiO_2	531.3	100			---	---
SiO_2@Sn^{+2}	531.1	44.3	529.6	40.3	533.8	15.4
SiO_2@nucAg	530.2	54.9	530.8	45.1	---	---
SiO_2@Ag	532.9	96.0	530.6	4.0	---	---

For SiO_2, SiO_2@Sn^{+2}, and SiO_2@nucAg the O 1s signal of Si-O at nearly 531 eV is observed.[24] But the SiO_2@Ag sample shows the typical signal of SiO_2 at nearly 533 eV, in complete agreement with the shift in the Si2p signal due to irradiation at 254 nm.[23] The shoulder at nearly 534 eV present in SiO_2@Sn^{+2} can be ascribed to (OH)-groups.[25] A signal at 529.9-529.8 eV, close to that observed here for SiO_2@Sn^{+2} (529.7 eV), was assigned to O bonded to Sn^{2+}.[26] The peaks at 530.2 eV for SiO_2@nucAg and at 530.6 eV for SiO_2@Ag were assigned to Sn-O.[27] Metallic silver nanoparticles typically show a $3d_{5/2}$ Ag peak at nearly 368 eV[8] in agreement with the signal at 367.9 eV obtained here for SiO_2@Ag. The lower binding energy of 366.0 eV detected here for SiO_2@nucAg was previously obtained for the emission of $3d_{5/2}$ photoelectrons from Ag^0 in nanoclusters.[27]

It is difficult to distinguish between Sn^{2+} and Sn^{4+} from XPS data.[9] However, from the observed peaks of Sn $3d_{5/2}$ at ca. 486 eV we can definitely exclude the presence of Sn^0 in samples SiO_2@Sn^{+2}, SiO_2@nucAg, and SiO_2@Ag.[9]

Figure 4 shows the extinction spectra of SiO_2, SiO_2@Sn^{2+}, SiO_2@AgNPs suspensions. The spectrum of aqueous suspensions of SiO_2@Ag shows the characteristic plasmon resonance band of silver nanoparticles with a maximum located at 432 nm.

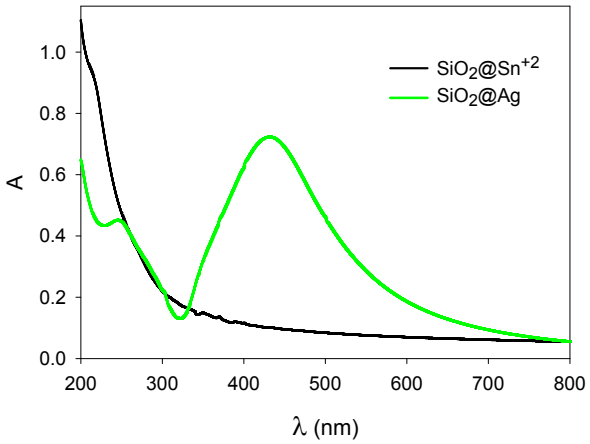

Figure 4: UV-visible extinction spectra of SiO_2@Sn^{2+} and SiO_2@Ag NPs suspensions as indicated.

Fluorescence correlation spectroscopy (FCS). From the time dependent fluorescence signals within the focal volume it is possible to obtain autocorrelation functions to yield the diffusion time of the fluorescent probe. From this information diffusion coefficients are calculated.

Care must be taken when performing FCS experiments with colloidal suspensions of nanoparticles because besides the fluorescence fluctuations detected with this technique, the Brownian motion of a single nanoparticle in a small highly focused detection volume (less than 1.0 fL) generates resonance light scattering fluctuations.[28] In fact, the detection of these fluctuations is the foundation of Resonance Light Scattering Correlation Spectroscopy (RLSCS). Since the translational diffusion model of fluorescent molecules in FCS can also be adopted in the diffusion model of metal nanoparticles in RLSCS, it is also possible to obtain diffusion coefficients from measurement of scattering fluctuations.[28]

For the above-given reasons, we here performed several FCS assays with suspensions of SiO_2@Ag NPs, solutions of the dyes and mixtures of both, in order to differentiate between signals arising from fluorescence and scattering. The criterion

employed for this distinction was based on signal intensity, which is expected to be much higher for fluorescence than for scattering effects.

FCS here is used to determine the degree of association of the dyes with the nanoparticles. By means of FCS is possible to distinguish between free dye, fast diffusing, and dye associated with the nanoparticles, which should diffuse more slowly. The autocorrelation functions obtained from FCS experiments (λ^{exc} = 458 nm; λ^{em} in the 500 - 570 nm range) performed with Rf solutions at a concentration of 9.3 µM at 37ºC were fit with a single component equation from which a diffusion coefficient D_{c1} = (485 ± 15) $\mu m^2 s^{-1}$ was retrieved. This value can be attributed to the diffusion of the free molecule in solution. Similar assays were also carried out with samples containing 9.3 µM of Rf and 13.905 to 41.715 µM of Ag in SiO_2@Ag. Under these conditions, the autocorrelation function was fit with a two-components equation highlighting the existence of a second fluorescent species with diffusion coefficient D_{c2} = (4.2 ± 0.4) $\mu m^2 s^{-1}$, which is related to diffusion of the dye absorbed on the NPs. Indeed, the sizes for the diffusing species calculated from the diffusion coefficient applying Stokes- Einstein is very similar to the sizes measured by TEM and DLS, confirming that the diffusion coefficient measured corresponds to the dye linked to the NP (Figure 5 and Table 2).

FCS experiments performed with the dye RB^{2-} did not yield good correlation diagram due to the low quantum yield of this dye.[29] Thus, it was not possible to employ the FCs technique with this dye to show binding to SiO_2@Ag NPs.

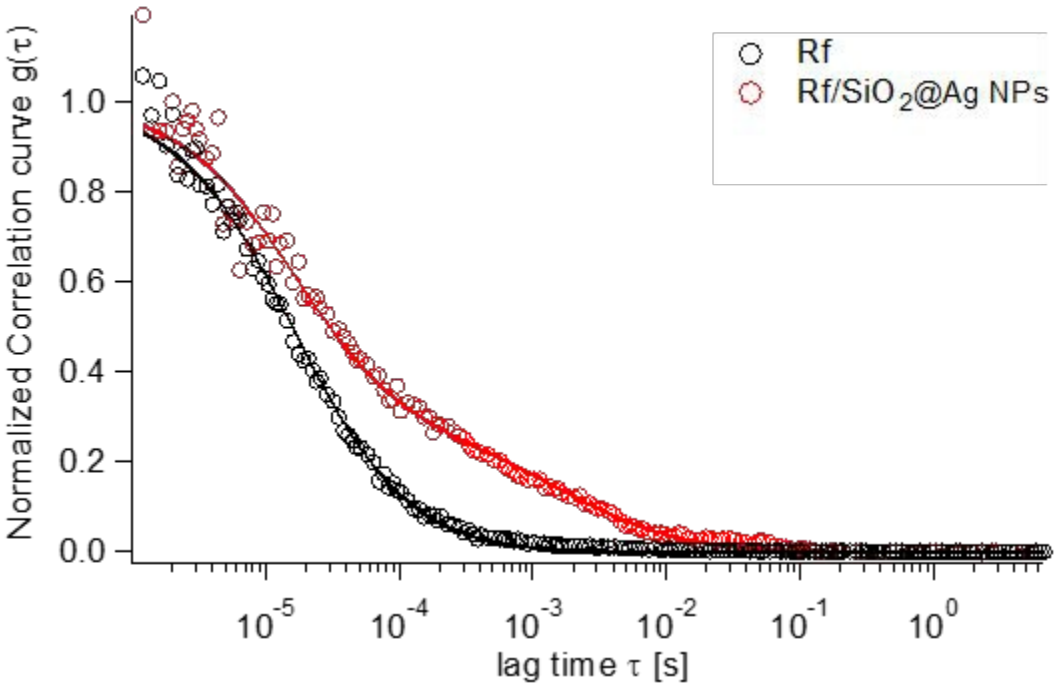

View Article Online
DOI: 10.1039/C9NJ01013K

Figure 5: Normalized autocorrelation curves of Riboflavin alone (black circles) and Riboflavin incubated with SiO_2@Ag NPs (red circles). Solid lines are the respective fits.

Table 2. FCS data obtained from the fitting of autocorrelation functions in Figure 6. The diffusion times (t_D) are obtained fitting the raw data by 3D-Normal Diffusion Model with 1 or 2 components. The confocal volume was estimated using 25 nM Rhodamine 6G.

	t_{D1} [μs]	t_{D2} [μs]	D_{c1}[μm²/s]	D_{c2} [μm²/s]
Rf	16.2 ± 0.5	-----	485 ± 15	-----
Rf/SiO_2@Ag*	16.2 ± 2.5	1886 ± 166	485 ± 75	4.2 ± 0.4

*Fitting is obtained fixing the diffusion time of the first component equivalent to the diffusion times of the free species.

Adsorption of the dyes on SiO_2@Ag and SiO_2. The chemical structure of the dyes is shown in Figure 6.

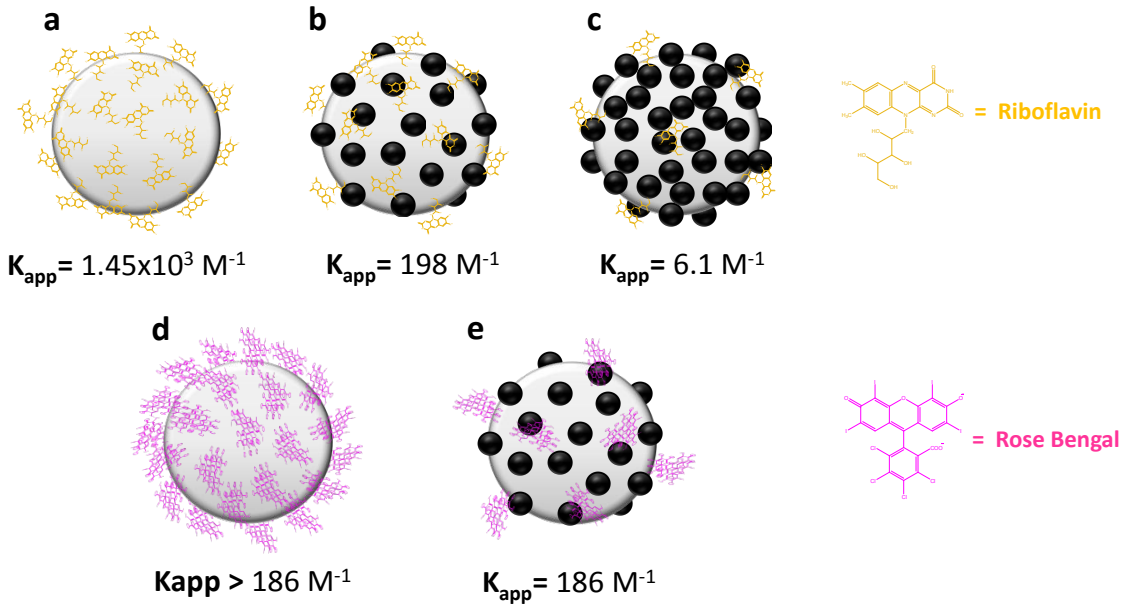

Figure 6 Scheme showing the adsorption of: (a) Rf on SiO_2 NPs; (b) Rf on SiO_2@Ag-low NPs; (c) Rf on SiO_2@Ag NPs; (d) RB^{2-} on SiO_2 NPs; (e) RB^{2-} on SiO_2@Ag-low NPs.

The absorption spectra of the dyes in the presence of increasing amounts of SiO_2@Ag are shown in Figures S3 - S4 in the Electronic Supporting Information. There is an enhanced absorption all over the evaluated wavelength range (200 - 800 nm). However, the increase of absorbance was wavelength dependent and after subtracting the contribution of the nanoparticles to the absorbance of the mixture the Benesi and Hildebrand eq I[30] was applied to obtain the apparent equilibrium constants (Kapp) for the complexation of the dyes with the nanoparticles.

$$\frac{1}{A - A_{dye}} = \frac{1}{A_C - A_{dye}} + \frac{1}{K_{app}(A_C - A_{dye})[NP]} \qquad (I)$$

In eq I A is the corrected absorbance at the analysis wavelength λ^{an} of the dye samples in the presence of different amounts of SiO_2 or SiO_2@Ag, and A_{dye} and A_c are the absorbances of the dye and the complex at λ^{an}, respectively. In order to be able to compare the data obtained with SiO_2 and SiO_2@Ag NPs, the insets of Figure S4 in the Electronic Supporting Information show the linear dependence of the left-hand side of eq I vs. the reciprocal of the silica concentration in the suspensions, $[SiO_2]^{-1}$ for Rf. The values of K_{app} obtained from the slopes and intercepts of the straight lines are shown in Table 3.

Table 3. Analysis wavelength λ^{an} and K_{app} values for the three dyes.

	$K_{app}(M^{-1})$
Rf[(a)]	
SiO_2	1.45×10^3
SiO_2@Ag-low[(b)]	198
SiO_2@Ag	6.1
RB[2-(c)]	
SiO_2@Ag	186

(a) Data obtained at λ^{an} = 440 nm. (b) Sample prepared employing a lower amount of the precursor $SnCl_2$. (c) Data obtained at λ^{an} = 400 nm.

Table 3 shows that for the adsorption of Rf the values of K_{app} follow the trend SiO_2 > SiO_2@Ag-low > SiO_2@Ag, which is indicative of the preference of Rf for the adsorption on SiO_2 sites compared to Ag. Figure 6 qualitatively shows this behavior. The absorption spectrum of RB^{2-} in the absence of nanoparticles (Figure 7a) shows a peak at 550 nm, which is characteristic of the monomer, with a shoulder at 510 nm assigned to the dimer.[31,32] Addition of even small amounts of SiO_2 NPs produces significant changes in the absorption spectra: the monomer band appears truncated, whereas the shoulder remains approximately constant (Figure S5 and Table S1). Thus, the presence of the nanoparticles leads to dimerization of the dye at the water/ silica interface. Similar experiments performed with SiO_2@Ag NPs instead of SiO_2 NPs (Figure 7a) show a gradual increase of the 510 shoulder with a concomitant decrease of the A^{550}/A^{510} ratio, as a measure of the dye aggregation (Figure 7b). These results show that aggregation is indicative of adsorption of RB^{2-} on the nanoparticles, and thus there is a lower affinity of the dye for SiO_2@Ag NPs than for SiO_2 NPs. The analysis of the spectra according to equation (I) for SiO_2 NPs yielded a high dispersion of the data irrespective of the wavelength chosen for analysis. However, for the interaction of RB^{2-} with SiO_2@Ag NPs it was possible to obtain the K_{app} of 186 at λ^{an} = 400 nm, a wavelength far from the monomer peak (550 nm) and dimer shoulder (510 nm). Figure 7c shows the Benesi-Hildebrandt plot.

In summary, both dyes Rf and RB^{2-} are preferentially adsorbed on SiO_2 sites (silanols), being the values of K_{app} for both dyes similar.

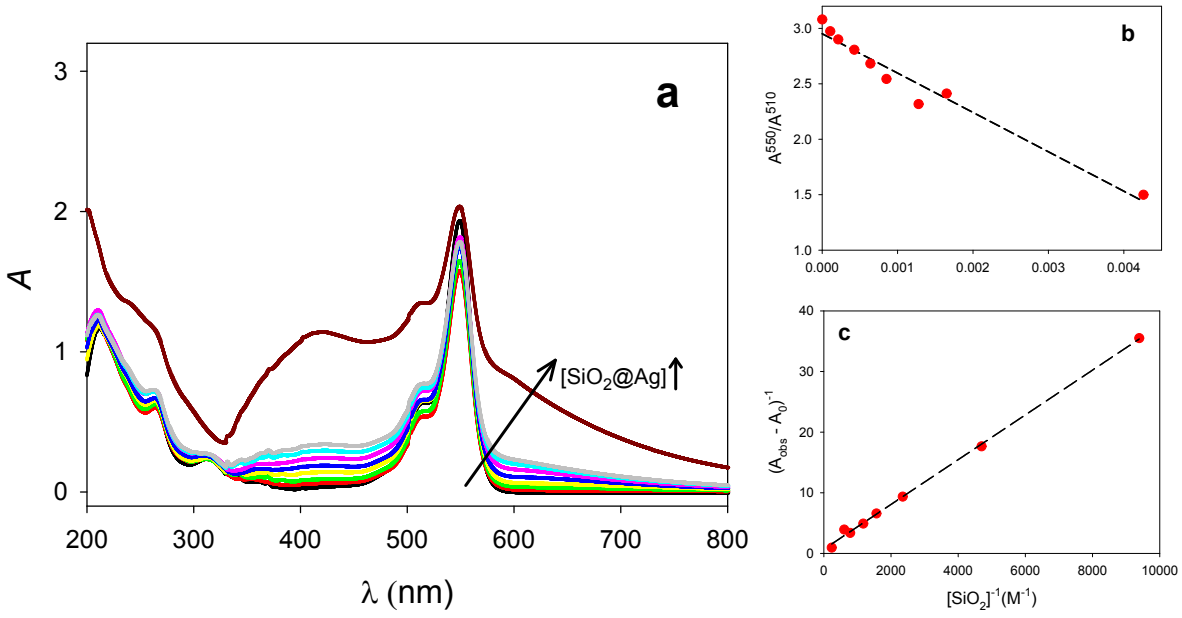

Figure 7:(a) UV-visible absorption spectra of a 29.4 μM solution of RB^{2-} in the presence of increasing amounts ofSiO_2@Ag NPs. (b). Plot of the ratio A^{510}/A^{550} as a measure of the dye aggregation vs. [Ag]. (c) Plot of $(A_{obs} - A_0)^{-1}$ vs $[Ag]^{-1}$ at400 nm for SiO_2@Ag NPs.

Laser Flash-Photolysis (LFP). Data obtained with Ar-saturated 27 μM Rf solutions in the absence of SiO_2@Ag NPs show positive values of ΔA in the 500-770 nm wavelength range employing a 0-40 μs time window. The photophysics of Rf is complex and thus, several species contribute to the observed signals, such as the triplet state (^{3}Rf*), its radical cation (Rf^{+}), and its neutral radical (HRf$^{\cdot}$), formed by fast protonation of the radical anion ($Rf^{\cdot-}$).[33]Due to the complexity of the system, the data were analyzed with the aid of the Glotaran program,[17] employing a sequential model with three species. Decay associated difference spectra (DADS) and lifetimes of each component were retrieved. Figure 8a shows the DADS of the species with the shortest lifetime (3.4 μs), which displays contributions of the spectra of ^{3}Rf* and Rf^{+}. The second species decays with a lifetime of 10.9 μs and has a DADS very similar to the absorption spectrum of Rf^{+} (Figure 8b), and is thus assigned to this radical ion.[33] The third species (Figure 8c) is attributed to HRf[33] and, as expected, decays with a longer lifetime (> 50 μs).

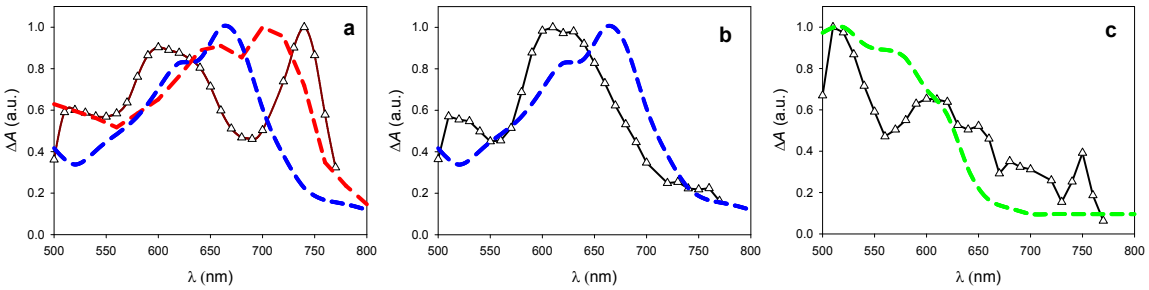

Figure 8: DADS corresponding to the lifetimes of: 3.4 μs (a), 10.9 μs (b), and > 1 ms (c), obtained from laser flash-photolysis experiments ([Rf] = 27 μM) under Ar-saturation after 355 nm excitation. The dashed lines represent the reported absorption spectra of ^{3}Rf* (red), Rf^{+} (blue), and HRf$^{\cdot}$ (green).[33]

The analysis with the Glotaran program of LFP signals obtained with 27 μM Rf (A^{355} = 0.5) samples prepared in suspensions of SiO_2@Ag-low NPs (0.301 μM ≤ [Ag] ≤ 1.81μM) also yielded three DADS. The spectrum with the shortest lifetime (15 - 40 ns) with negative contributions in the whole wavelength range, is ascribed to the electronic response of our LFP set-up to scattering of the samples. The second DADS (see Figure 9a) had a lifetime of 9 μs. This DADS is very similar to the reported absorption spectrum of $Rf^{\bullet+}$ and is assigned to this radical. The third species, assigned to $HRf^{\bullet}$ (Figure 9b) displayed longer lifetime (> 50 μs).

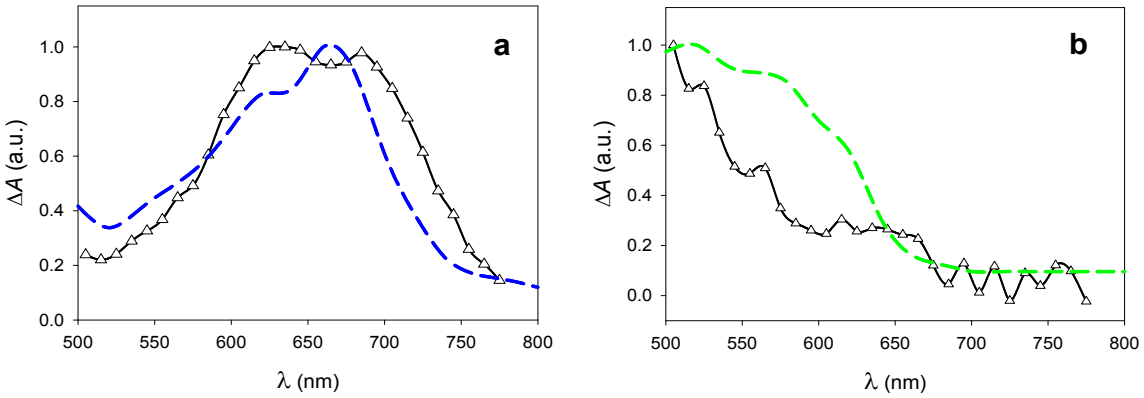

Figure 9: DADS corresponding to Rf species in the presence of SiO_2@Ag-low NPs: $Rf^{\bullet+}$ (a) and $HRf^{\bullet}$ (b) obtained from laser flash-photolysis experiments under Ar-saturation after 355 nm excitation. Experiments performed with [Rf] = 27 μM and [Ag] = 3.6×10^{-6}M. The dashed lines represent the reported absorption spectra of $Rf^{\bullet+}$ (blue), and $HRf^{\bullet}$ (green).[33]

The reason why the triplet state of Rf is not observed in the presence of SiO_2@Ag-low NPs could be the occurrence of an efficient charge transfer from the silver nanoparticles to the singlet excited state of Rf (^{1}Rf*) (reaction 2). The competition of this reaction with the intersystem crossing process (3) precludes the detection of ^{3}Rf* in the LFP assays.

$$^1Rf^* + Ag \rightarrow Rf^{\bullet-} + Ag^+ \qquad (2)$$

$$^1Rf^* \rightarrow {}^3Rf^* \qquad (3)$$

Reaction (2) is thermodynamically feasible, as indicated by the Gibbs energy calculated from the Rehm-Weller equation[34]: $\triangle_{ET}G^o$ = -111 kJ/mol. The existence of this reaction implies a decrease of the singlet state lifetime (τ_s) in the presence of the nanoparticles. However, τ_s was not affected by the nanoparticles (see Table S2 in the Supplementary Material).

View Article Online
DOI: 10.1039/C9NJ01013K

These results support the idea that the charge transfer from silver nanoparticles to the excited singlet state of Rf in solution (^{1}Rf*) is not the responsible for the absence of the triplet signal in the LFP assays performed with SiO_2@Ag-low NPs. A plausible explanation involves the charge transfer reaction (4) from Ag to the excited state of the non-fluorescent complex between Rf and the nanoparticles (*Rf-NP).

$$*\text{Rf-NP} + \text{Ag} \leftrightarrows \text{Rf}^{\cdot-}\text{-NP} + \text{Ag}^{+} \qquad (4)$$

Rf$^{\cdot-}$-NP represents the adsorbed radical anion of Rf.

From reaction 4, we can conclude that the presence of Rf and further laser excitation will induce the generation of Ag^+ ions, which can have interesting antimicrobial applications.

In order to investigate the effect of the degree of silver coverage on the silica surface, another series of LFP experiments were performed with Rf in the presence of SiO_2@Ag NPs with higher Ag content. Surprisingly, in this case the results were different from those obtained with SiO_2@Ag-low NPs. The Glotaran analysis yielded three species with DADS and kinetics similar to the data shown in Figure 8 (see Figure S6 in the Electronic Supporting Information). The species with the shortest lifetime (11.50 ns) can be assigned to a scattering component. The second species with a lifetime of 12.54 μs shows unambiguous contribution of ^{3}Rf*. This result is in line with the lower affinity of Rf for the core-shell NPs with lower amounts of surface silanol groups, which disfavors the occurrence of reaction (4). The third component (99.68 μs) can be assigned to the radical cation of Rf.

LFP experiments were performed with RB^{2-} samples in the presence and absence of SiO_2@Ag NPs in the wavelength ranges 580- 700 nm and 350- 480 nm. In the former region the only transient species absorbing in the time window of our experiments is the triplet state of the dye, $^3RB^{2-}$*. In the shorter wavelengths region the triplet state also absorbs along with the semi-reduced radical ($RB^{\cdot 3-}$) and semi-oxidized ($RB^{\cdot-}$) radicals. These radicals are formed through disproportionation of the triplet state and ground state of RB (RB^{2-}).[35]

$$^3\text{RB}^{2-}* + \text{RB}^{2-} \rightarrow \text{RB}^{\cdot-} + \text{RB}^{\cdot 3-} \qquad (5)$$

Global analysis of the experiments performed under Ar saturation in the 580- 700 nm range showed the contribution of only one species with a lifetime of 10 ± 2 μs and an absorption spectrum coincident with that of $^3RB^{2-}$* (Figure 10a). Both the lifetime and the spectrum were independent of the presence of SiO_2@Ag-low NPs. In the 350 - 480 nm range the program detected three components: the lifetime of the first component was again 10 ± 2 μs and the DADS showed positive

View Article Online
DOI: 10.1039/C9NJ01013K

absorption in the absence of the particles, whereas a negative region at around 430 nm appeared in the presence of SiO_2@Ag NPs. We should here stress that with the LFP technique differential spectra are obtained, i.e, the measured ΔA values are the difference between the absorbance of the triplet state and that of the unexcited sample. Thus, in the 350 - 480 nm region and in the absence of SiO_2@Ag-low NPs, the absorption of the triplet is larger than that of the ground-state and $\Delta A > 0$. When the SiO_2@Ag NPs are present the plasmon absorption contributes to the negative component of ΔA in the region at around 420 nm. As can be seen in Figure 10b, this negative contribution increases with increasing amounts of nanoparticles in the samples. All these results support the assignment of the first component to $^3RB^{2-}$*.

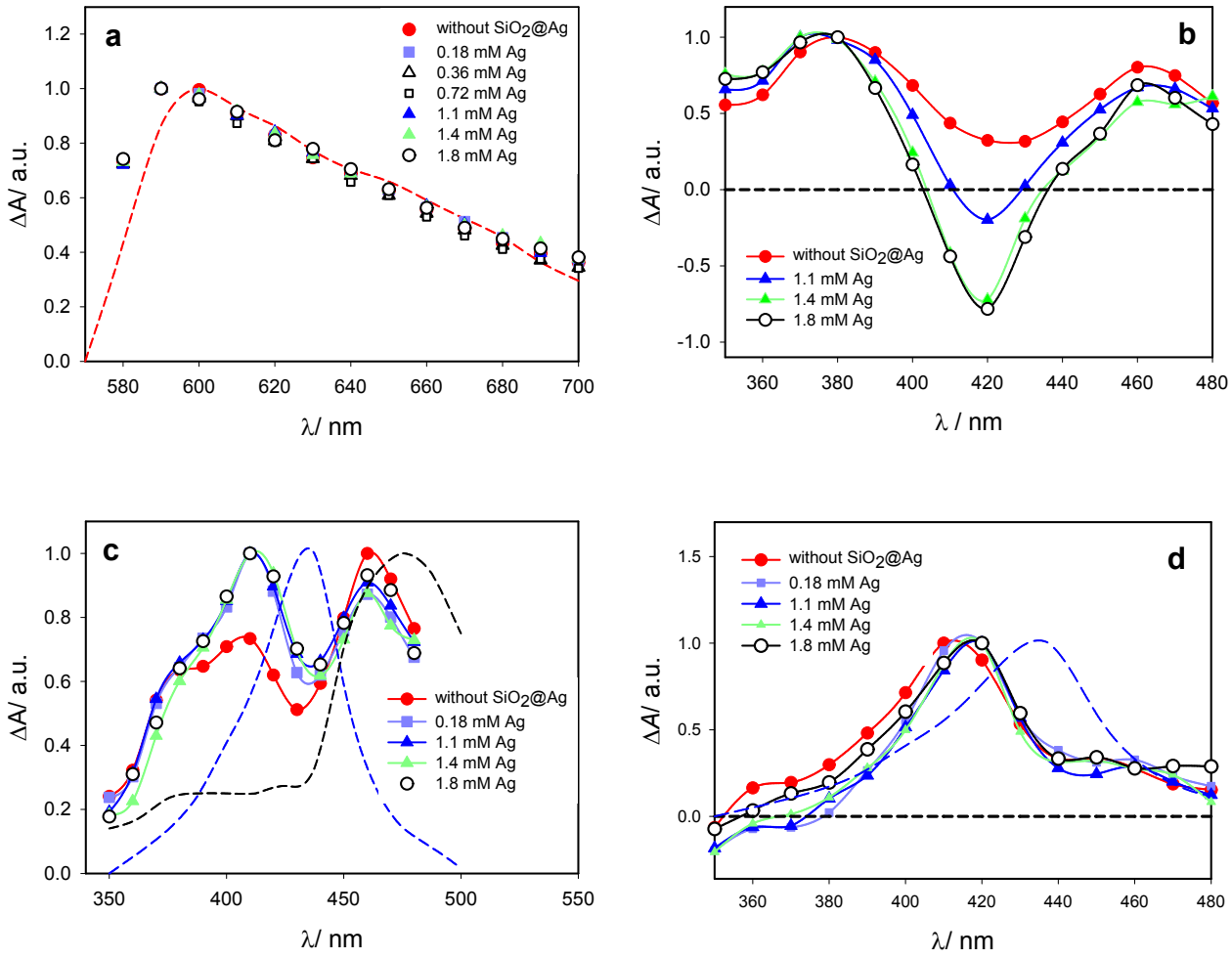

Figure 10: DADS corresponding to Rose Bengal species in the absence and presence of SiO_2@Ag NPs: the first component assigned to $^3RB^{2-}$* (a and b); the second component (c) and the third component (d) obtained from photolysis experiments under Ar-saturation after 355 nm excitation. Experiments performed with $[RB^{2-}]$ = 147 μM and various amounts of Ag in

View Article Online
DOI: 10.1039/C9NJ01013K

SiO_2@Ag NPs as indicated. The dashed lines represent the reported absorption spectra of $^3RB^{2-}$* (red), $RB^{\bullet-}$ (black) $RB^{\bullet 3-}$ (blue).

The second component with a lifetime of 23 ± 8 μs shows a DADS with contributions of $RB^{\bullet-}$ and $RB^{\bullet 3-}$ radicals (Figure 10c), whereas the DADS of the third component with a lifetime of 239 ± 37 μs is coincident with that assigned to $RB^{\bullet 3-}$ (Figure 10d). [36] These results are in line with the longer lifetime reported for the semi-reduced radical $RB^{\bullet 3-}$ compared to $RB^{\bullet-}$.[36]

Glotaran analysis of data obtained from LFP experiments performed with RB^{2-} samples in the presence and absence of SiO_2@Ag-low NPs in the wavelength ranges 580- 700 nm under air-saturation yielded one component with a lifetime of 2.15 ± 0.03 μs. From this lifetime, the triplet decay obtained in Ar-saturated samples (10 μs), and the concentration of molecular oxygen in air-saturated solutions (0.29 mM)[37], a quenching rate constant of $^3RB^{2-}$* by oxygen of 1.3×10^9 $M^{-1}s^{-1}$ is obtained, in excellent agreement with the reported value of 1.6×10^9 $M^{-1}s^{-1}$.[38]The DADS were also coincident with the reported spectrum of the triplet state (result not shown).

In summary, although RB^{2-} adsorbs on SiO_2@Ag-low NPs, no effect of the nanoparticles could be observed on the triplet state of the dye could be observed.

Comparison of the data obtained with both dyes indicate that Rf and RB^{2-} are more favorably adsorbed on SiO_2 NPs, showing preference for the silanol groups of the nanoparticles compared to the metal sites. The apparent rate constants K_{app} obtained for the complexation are similar. When nanoparticles with a low coverage of silver (SiO_2@Ag-low NPs) were employed in LFP assays, it was not possible to observe the absorption of the excited triplet state of Rf (^{3}Rf*) and this behavior was explained by a charge transfer reaction from Ag to the excited state of the non-fluorescent complex between Rf and the nanoparticles (*Rf-NP) (reaction 4). However, neither the amount nor the decay of the triplet state of Rose Bengal ($^3RB^{2-}$*) were affected by the presence of SiO_2@Ag-low NPs. This result indicates that the complex of this dye with the nanoparticles (*RB^{2-}-NP) is not prone to transfer electrons to the silver nanoparticles in a reaction similar to reaction (4). These results are explained in terms on the feasibility of the one-electron transfer from the nanoparticles to triplet states of both dyes.

View Article Online
DOI: 10.1039/C9NJ01013K

Table 4 lists the values of the triplet state energy (E_T), ground state and triplet state redox potentials of the sensitizers, and the Gibbs energy ($\Delta_{ET}G^o$) and equilibrium constants for the one-electron transfer process (6) for $^3S^* = {}^3Rf^*$ or $^3RB^{2-*}$.

$$^3S^* + Ag \rightarrow S^{\bullet-}\text{-NP} + Ag^+ \qquad (6)$$

Table 4. Triplet state energy (E_T), ground- and triplet state redox potential of the sensitizers, Gibbs energy ($\Delta_{ET}G^o$) and equilibrium constants (K) of reaction (6) for S = RB^{2-} and Rf.

S	E_T/kJ·mol^{-1}	Ground State Redox Potential vs. NHE/ V	Triplet State Redox Potential vs. NHE/ V	$\Delta_{ET}G^o$/kJ mol^{-1}[a]	K
RB^{2-}	175.6 [b]	E^o ($RB^{2-}/RB^{\cdot 3-}$) = -0.78 [c]	E^o ($^3RB^{2-*}/RB^{\cdot 3-}$) = 1.04 [b]	-25.1	2.5×10^4
Rf	209 [d]	E^o ($Rf/Rf^{\cdot -}$) = -0.546 [e]	E^o ($^3Rf^*/Rf^{\cdot -}$) = 1.62 [f]	-81.0	1.6×10^{14}

[a] Calculated from the Rehm-Weller equation[34] taking 0.78 V for the redox potential E^o (Ag^+/Ag) vs. NHE, which is the value reported for silver nanoparticles of about 10 nm diameter diameter.[39] [b] From[35]. [c] From [40]. [d] From [41]. [e] From [42]. [f] From[6].

Assuming that the triplet state redox potentials of the sensitizers are similar when they are free or adsorbed on the nanoparticles, we can predict that reaction (7), a thermodynamically feasible process, has an equilibrium constant K ten orders of magnitude lower than reaction (4). This should be the reason why no effect of SiO_2@Ag-low NPs on the triplet state of Rose Bengal is observed, whereas the nanoparticles had a drastic quenching effect on the triplet state of Rf.

$$^*RB^{2-}\text{-NP} + Ag \leftrightarrows RB^{\cdot 3-}\text{-NP} + Ag^+ \qquad (7)$$

It is also noteworthy that although RB^{2-} dimerizes on the surface of SiO_2 NPs, our transient absorption assays clearly show that the dimer dissociates in the triplet excited state, in complete coincidence with reported data on the excited states of

RB^{2-} on silica surfaces.[42] This agreement supports the absence under our experimental conditions of any effect of the silver nanoparticles on the photophysics of RB^{2-}.

CONCLUSION

We have here synthesized novel core-shell SiO_2@Ag nanoparticles by a two steps method, which involves the homogeneous deposition of silver nuclei on colloidal silica spheres followed by a photochemical method employed for the growth of silver nanoparticles from silver seeds.

Nanoparticles were characterized by several methods and their interaction with the ground-states and excited triplet states of Rose Bengal and Riboflavin, two typical photosensitizers with photodynamic activity, were investigated. Both dyes were shown to be adsorbed on the nanoparticles. Transient absorption spectroscopy experiments showed that in samples containing Rf and SiO_2@Ag-low NPs, the absorption of the triplet excited state of Riboflavin is not observed because of an electron transfer process from Ag to the excited state of the complex formed between Rf and SiO_2 nanoparticles. This result means that under these conditions upon photoirradiation Ag^+ are released to the aqueous medium (see Figure 11).

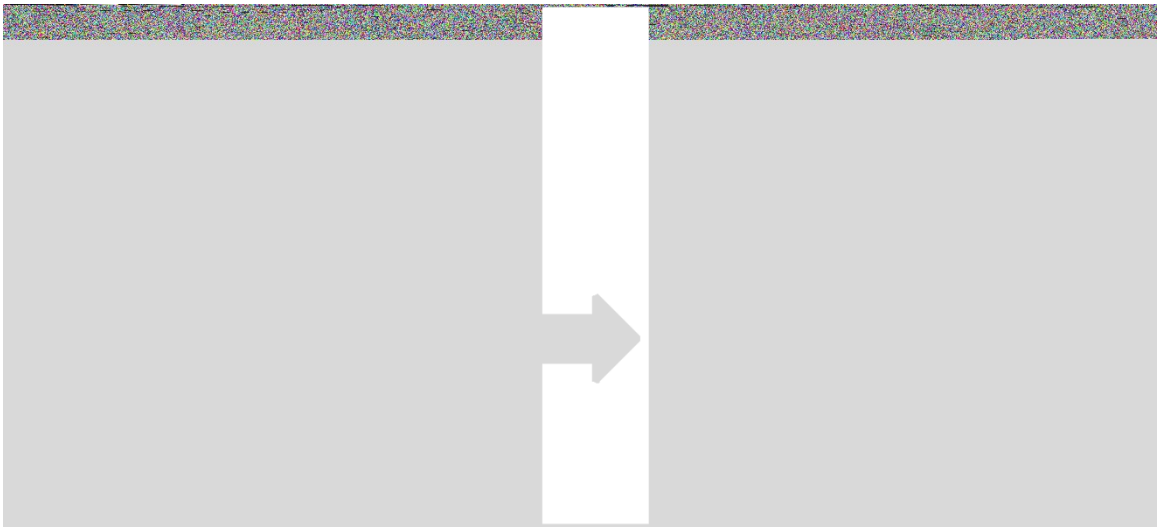

Figure 11: Schematic picture of the photoinduced release of Ag^+ from samples containing Rf and SiO2@Ag-low NPs.

However, no effect of SiO_2@Ag-low NPs on the triplet excited state of Rose Bengal was observed, being the electron transfer much less favorable in this case.

It is accepted that the localized release of Ag^+ ions at the cell walls of microorganisms contributes to the antibacterial activity of the silver nanomaterials.[43,44] For this reason, our core-shell SiO_2@Ag-low NPs are promising candidates for the

photodynamic inactivation (PDI) of microorganisms. Photoirradiation of Riboflavin in suspensions of the nanoparticles should release Ag^+ ions, enhancing the intrinsic antibacterial effect of the non-irradiated nanomaterials.

CONFLICTS OF INTEREST

There are no conflicts of interest to declare.

ACKNOWLEDGMENTS

This work has been supported by grant PICT 2016-0974 from ANPCyT, Argentina. J.E.M.P. and M.B.R.A. thank CONICET for graduate studentships. V.B.A. and D.O.M. are research members of CIC, Buenos Aires, Argentina. We thank Dr. Luis Yate for the XPS measurements.

REFERENCES

(1) Aslan, K.; Gryczynski, I.; Malicka, J.; Matveeva, E.; Lakowicz, J. R.; Geddes, C. D. Metal-Enhanced Fluorescence: An Emerging Tool in Biotechnology. *Curr. Opin. Biotechnol.* **2005**, *16* (1 SPEC. ISS.), 55–62. https://doi.org/10.1016/j.copbio.2005.01.001.

(2) Pacioni, N. L.; González-Béjar, M.; Alarcón, E.; McGilvray, K. L.; Scaiano, J. C.; González-Béjar, M.; Alarcón, E.; McGilvray, K. L.; Scaiano, J. C. Surface Plasmons Control the Dynamics of Excited Triplet States in the Presence of Gold Nanoparticles. *J. Am. Chem. Soc* **2010**, *132* (18), 6298–6299. https://doi.org/10.1021/ja101925d.

(3) Morton, S. M.; Silverstein, D. W.; Jensen, L. Theoretical Studies of Plasmonics Using Electronic Structure Methods. **2011**, 3962–3994. https://doi.org/10.1021/cr100265f.

(4) Yang, W.; Liu, K.; Song, D.; Du, Q.; Wang, R.; Su, H. Aggregation-Induced Enhancement E Ff Ect of Gold Nanoparticles on Triplet Excited State. **2013**. https://doi.org/10.1021/jp410369w.

(5) Planas, O.; Macia, N.; Agut, M.; Nonell, S.; Heyne, B. Distance-Dependent

Plasmon-Enhanced Singlet Oxygen Production and Emission for Bacterial Inactivation. *J. Am. Chem. Soc.* **2016**, *138* (8), 2762–2768. https://doi.org/10.1021/jacs.5b12704.

(6) Rivas Aiello, M. B.; Romero, J. J.; Bertolotti, S. G.; Gonzalez, M. C.; Mártire, D. O. Effect of Silver Nanoparticles on the Photophysics of Riboflavin: Consequences on the ROS Generation. *J. Phys. Chem. C* **2016**, *120* (38). https://doi.org/10.1021/acs.jpcc.6b06385.

(7) Nanoparticles, P. S.; Aiello, R.; Castrogiovanni, D.; Parisi, J.; Azc, J. C.; Garc, F. S.; Gensch, T.; Bosio, G. N.; Daniel, O. M. Photodynamic Therapy in HeLa Cells Incubated with Ribo Fl Avin And. No. 19, 1–8. https://doi.org/10.1111/php.12974.

(8) Gun'ko, V. M.; Turov, V. V.; Zarko, V. I.; Goncharuk, O. V.; Pakhlov, E. M.; Skubiszewska-Zięba, J.; Blitz, J. P. Interfacial Phenomena at a Surface of Individual and Complex Fumed Nanooxides. *Adv. Colloid Interface Sci.* **2016**, *235*, 108–189. https://doi.org/10.1016/j.cis.2016.06.003.

(9) Kobayashi, Y.; Salgueiriño-Maceira, V.; Liz-Marzán, L. M. Deposition of Silver Nanoparticles on Silica Spheres by Pretreatment Steps in Electroless Plating. *Chem. Mater.* **2001**, *13* (5), 1630–1633. https://doi.org/10.1021/cm001240g.

(10) McGilvray, K. L.; Fasciani, C.; Bueno-Alejo, C. J.; Schwartz-Narbonne, R.; Scaiano, J. C. Photochemical Strategies for the Seed-Mediated Growth of Gold and Gold-Silver Nanoparticles. *Langmuir* **2012**, *28* (46), 16148–16155. https://doi.org/10.1021/la302814v.

(11) Scaiano, J. C.; Billone, P.; Gonzalez, C. M.; Marett, L.; Marin, M. L.; McGilvray, K. L.; Yuan, N. Photochemical Routes to Silver and Gold Nanoparticles. *Pure Appl. Chem.* **2009**, *81* (4), 635–647. https://doi.org/10.1351/pac-con-08-09-11.

(12) Al-Akhras, M. A. H.; Aljarrah, K.; Albiss, B.; Al-Khalili, D. Influence of Iron Oxide Nanoparticles (Fe3O4) on Erythrocyte Photohemolysis via Photofrin and Rose Bengal Sensitization. *Photodiagnosis Photodyn. Ther.* **2017**, *18*, 111–118. https://doi.org/10.1016/j.pdpdt.2017.02.008.

(13) Halili, F.; Arboleda, A.; Durkee, H.; Taneja, M.; Miller, D.; Alawa, K. A.; Aguilar, M. C.; Amescua, G.; Flynn, H. W.; Parel, J. M. Rose Bengal- and Riboflavin-Mediated Photodynamic Therapy to Inhibit Methicillin-Resistant Staphylococcus Aureus Keratitis Isolates. *Am. J. Ophthalmol.* **2016**, *166*, 194–202. https://doi.org/10.1016/j.ajo.2016.03.014.

(14) Bacellar, I. O. L.; Tsubone, T. M.; Pavani, C.; Baptista, M. S. Photodynamic Efficiency: From Molecular Photochemistry to Cell Death. *Int. J. Mol. Sci.* **2015**, *16* (9), 20523–20559. https://doi.org/10.3390/ijms160920523.

(15) Stober, W.; Fink, A. Controlled Growth of Monodispersed Silica Spheres in the Micron Size Range. *J. Colloid Interface Sci.* **1968**, *26*, 62–69.

(16) Westcott, S. L.; Oldenburg, S. J.; Lee, T. R.; Halas, N. J. Formation and Adsorption of Clusters of Gold Nanoparticles onto Functionalized Silica Nanoparticle Surfaces. *Langmuir* **1998**, *14* (19), 5396–5401. https://doi.org/10.1021/la980380q.

(17) Snellenburg, J. J.; Laptenok, S. P.; Seger, R.; Mullen, K. M.; van Stokkum, I. H. M. Glotaran : A Java -Based Graphical User Interface for the R Package TIMP. *J. Stat. Softw.* **2012**, *49* (3). https://doi.org/10.18637/jss.v049.i03.

(18) Tzounis, L.; Contreras-Caceres, R.; Schellkopf, L.; Jehnichen, D.; Fischer, D.; Cai, C.; Uhlmann, P.; Stamm, M. Controlled Growth of Ag Nanoparticles Decorated onto the Surface of SiO_2 Spheres: A Nanohybrid System with Combined SERS and Catalytic Properties. *RSC Adv.* **2014**, *4* (34), 17846–17855. https://doi.org/10.1039/C4RA00121D.

(19) Merga, G.; Wilson, R.; Lynn, G.; Milosavljevic, B. H.; Meisel, D. Redox Catalysis on “Naked” Silver Nanoparticles. *J. Phys. Chem. C* **2007**, *111* (33), 12220–12226. https://doi.org/10.1021/jp074257w.

(20) Himpsel, F. J.; McFeely, F. R.; Taleb-Ibrahimi, A.; Yarmoff, J. A.; Hollinger, G. Microscopic Structure of the SiO2/Si Interface. *Phys. Rev. B* **1988**, *38* (9), 6084–6096. https://doi.org/10.1103/PhysRevB.38.6084.

(21) Logofatu, C.; Negrila, C. C.; Ghita, R. V; Ungureanu, F.; Cotirlan, C.; Lazarescu, C.

G. A. S. M. and M. F. Study of SiO 2 / Si Interface by Surface Techniques. *Cryst. Silicon - Prop. Uses Ed. by Prof. Sukumar Basu* **2011**, *1* (100), 2–42. https://doi.org/10.5772/844.

(22) Önneby, C.; Pantano, C. G. Silicon Oxycarbide Formation on SiC Surfaces and at the SiC/SiO2 Interface. *J. Vac. Sci. Technol. A Vacuum, Surfaces, Film.* **1997**, *15* (3), 1597–1602. https://doi.org/10.1116/1.580951.

(23) Aminuzzaman, M.; Watanabe, A.; Miyashita, T. Photochemical Surface Modification and Characterization of Double-Decker-Shaped Polysilsesquioxane Hybrid Thin Films. *J. Mater. Chem.* **2008**, *18* (42), 5092. https://doi.org/10.1039/b809819k.

(24) Shen, T. D.; Shmagin, I.; Koch, C. C.; Kolbas, R. M.; Fahmy, Y.; Bergman, L.; Nemanich, R. J.; McClure, M. T.; Sitar, Z.; Quan, M. X. Photoluminescence from Mechanically Milled Si and SiO2 Powders. *Phys. Rev. B* **1997**, *55* (12), 7615–7623. https://doi.org/DOI 10.1103/PhysRevB.55.7615.

(25) Zatsepin, D. A.; Zatsepin, A. F.; Boukhvalov, D. W.; Kurmaev, E. Z.; Gavrilov, N. V. Sn-Loss Effect in a Sn-Implanted a-SiO2host-Matrix after Thermal Annealing: A Combined XPS, PL, and DFT Study. *Appl. Surf. Sci.* **2016**, *367*, 320–326. https://doi.org/10.1016/j.apsusc.2016.01.126.

(26) Kwoka, M.; Ottaviano, L.; Passacantando, M.; Santucci, S.; Czempik, G.; Szuber, J. XPS Study of the Surface Chemistry of L-CVD SnO2thin Films after Oxidation. *Thin Solid Films* **2005**, *490* (1), 36–42. https://doi.org/10.1016/j.tsf.2005.04.014.

(27) Gao, S.; Chen, D.; Li, Q.; Ye, J.; Jiang, H.; Amatore, C.; Wang, X. Near-Infrared Fluorescence Imaging of Cancer Cells and Tumors through Specific Biosynthesis of Silver Nanoclusters. *Sci. Rep.* **2014**, *4*, 1–6. https://doi.org/10.1038/srep04384.

(28) Zhang, B.; Liu, H.; Huang, X.; Dong, C.; Ren, J. Size Distribution of Nanoparticles in Solution Characterized by Combining Resonance Light Scattering Correlation Spectroscopy with the Maximum Entropy Method. *Anal. Chem.* **2017**, *89* (22), 12609–12616. https://doi.org/10.1021/acs.analchem.7b04166.

(29) Estrada, L. C.; Aramendía, P. F.; Martínez, O. E. 10000 Times Volume Reduction for Fluorescence Correlation Spectroscopy Using Nano-Antennas. **2008**, *16* (25), 20597–20602.

(30) Benesi, B. A. California] A Spectrophotometric Investigation of the Interaction of Iodine with Aromatic Hydrocarbons. **1949**, *2832* (1948). https://doi.org/10.1021/ja01176a030.

(31) Doktorovova, S.; Shegokar, R.; Martins-Lopes, P.; Silva, A. M.; Lopes, C. M.; Müller, R. H.; Souto, E. B. Modified Rose Bengal Assay for Surface Hydrophobicity Evaluation of Cationic Solid Lipid Nanoparticles (CSLN). *Eur. J. Pharm. Sci.* **2012**, *45* (5), 606–612. https://doi.org/10.1016/j.ejps.2011.12.016.

(32) Rauf, M. A.; Graham, J. P.; Bukallah, S. B.; Al-Saedi, M. A. S. Solvatochromic Behavior on the Absorption and Fluorescence Spectra of Rose Bengal Dye in Various Solvents. *Spectrochim. Acta - Part A Mol. Biomol. Spectrosc.* **2009**, *72* (1), 133–137. https://doi.org/10.1016/j.saa.2008.08.018.

(33) Li, H.; Melø, T. B.; Razi Naqvi, K. Triplets, Radical Cations and Neutral Semiquinone Radicals of Lumiflavin and Riboflavin: An Overhaul of Previous Pump-Probe Data and New Multichannel Absolute Absorption Spectra. *J. Photochem. Photobiol. B Biol.* **2012**, *106* (1), 34–39. https://doi.org/10.1016/j.jphotobiol.2011.10.003.

(34) Edition, T. *Principles of Fluorescence Spectroscopy*.

(35) Ludvíková, L.; Friš, P.; Heger, D.; Šebej, P.; Wirz, J.; Klán, P. Photochemistry of Rose Bengal in Water and Acetonitrile: A Comprehensive Kinetic Analysis. *Phys. Chem. Chem. Phys.* **2016**, *18* (24), 16266–16273. https://doi.org/10.1039/C6CP01710J.

(36) Lambert, C.; Sarna, T.; Truscott, T. G. Rose Bengal Radicals and Their Reactivity. *J. Chem. Soc. Faraday Trans.* **1990**, *86* (23), 3879–3882. https://doi.org/10.1039/ft9908603879.

(37) Eggeling, C.; Widengren, J.; Rigler, R.; Seidel, C. A. M. Photostability of

Fluorescent Dyes for Single-Molecule Spectroscopy: Mechanisms and Experimental Methods for Estimating Photobleaching in Aqueous Solution. *Appl. Fluoresc. Chem. Biol. Med.* **1999**, 193–240. https://doi.org/10.1007/978-3-642-59903-3_10.

(38) Lee, P. C. C.; Rodgers, M. A. J. Laser Flash Photokinetic Studies of Rose Bengal Sensitized Photodynamic Interactions of Nucleotides and Dna. *Photochem. Photobiol.* **1987**, *45* (1), 79–86. https://doi.org/10.1111/j.1751-1097.1987.tb08407.x.

(39) Ivanova, O. S.; Zamborini, F. P. Size-Dependent Electrochemical Oxidation of Silver Nanoparticles. **2010**, 70–72.

(40) Lambert, C. R.; Kochevar, I. E. Electron Transfer Quenching of the Rose Bengal Triplet State. *Photochem. Photobiol.* **1997**, *66* (1), 15–25. https://doi.org/10.1111/j.1751-1097.1997.tb03133.x.

(41) Porcal, G.; Bertolotti, S. G.; Previtali, C. M.; Encinas, M. V. Electron Transfer Quenching of Singlet and Triplet Excited States of Flavins and Lumichrome by Aromatic and Aliphatic Electron Donors. *Phys. Chem. Chem. Phys.* **2003**, *5* (19), 4123. https://doi.org/10.1039/b306945a.

(42) Tan, S. L. J.; Webster, R. D. Electrochemically Induced Chemically Reversible Proton-Coupled Electron Transfer Reactions of Riboflavin (Vitamin B 2). **2012**. https://doi.org/10.1021/ja300191u.

(43) Xiu, Z.; Zhang, Q.; Puppala, H. L.; Colvin, V. L.; Alvarez, P. J. J. Negligible Particle-Speci Fi c Antibacterial Activity of Silver Nanoparticles. **2012**, 10–14. https://doi.org/10.1021/nl301934w.

(44) Richter, A. P.; Brown, J. S.; Bharti, B.; Wang, A.; Gangwal, S.; Houck, K.; Hubal, E. A. C.; Paunov, V. N.; Stoyanov, S. D.; Velev, O. D. Nanoparticle Based on a Silver-Infused Lignin Core. *Nat. Nanotechnol.* **2015**, *10* (9), 817–823. https://doi.org/10.1038/nnano.2015.141.